Journal of Applied Polymer Science

Enhanced Interfacial Interaction of Epoxy Nanocomposites with Activated Graphene Nanosheets

Hui Deng, Fan Wu, Lei Chen, Zhiwei Xu, Liangsen Liu, Caiyun Yang, Wei Mai, Bowen Cheng
Key Laboratory of Advanced Braided Composites, Ministry of Education, Nonwoven Materials and Engineering Department, School of Textiles, Tianjin Polytechnic University, Tianjin 300160, People's Republic of China
Correspondence to: L. Liu (E-mail: 83019163@163.com)

ABSTRACT: The interfacial properties of epoxy nanocomposites reinforced by thermally exfoliated graphene nanosheets (TEG) and activated thermally exfoliated graphene nanosheets (a-TEG) were compared. The specific surface area (SSA) of a-TEG with well-defined micro-mesopore size distribution was 1000 m^2/g, which was much higher that of TEG (550 m^2/g). The interfacial interaction between a-TEG and epoxy was stronger than that of TEG/epoxy owing to their higher SSA and pore size which was proved by dynamic mechanical analysis. As a result, the tensile strength of a-TEG/epoxy was increased compared with that of TEG/epoxy for all concentrations. In particular, the tensile and flexural strength of a-TEG/epoxy was increased up to 20 and 50% in comparison to that of TEG/epoxy at 0.05 wt % graphene, respectively. © 2014 Wiley Periodicals, Inc. J. Appl. Polym. Sci. **2014**, *131*, 41164.

KEYWORDS: composites; fullerenes; graphene; mechanical properties; nanotubes

Received 27 February 2014; accepted 14 June 2014
DOI: 10.1002/app.41164

INTRODUCTION

Graphene-based polymer nanocomposites have recently received much attention due to the unique mechanical, electrical, and thermal properties of graphene.[1–4] It has been demonstrated that the Young's modulus and tensile strength of nanocomposites at only 0.1 wt % graphene were increased by 31 and 40% compared with the neat epoxy.[5] However, the homogeneous dispersion and efficient interfacial interactions are still the main challenges for graphene nanocomposites.[6,7] On one hand, much effort was focused on the chemical functionalization of reinforcements to improve the chemical bonding between reinforcements and matrix.[8–10] On the other hand, some researches indicated that the proper geometrical design of reinforcements can effectively strengthen the mechanical junctions of composites.[11–13]

It has been demonstrated that the large surface area of graphene could increase the contact area with the polymer matrix and make the stress transfer from the polymer to the nanoplatelets effectively, resulting in a pronounced effect on the mechanical properties and thermal conductivity of epoxy composites.[13–15] Therefore, a proper geometrical design of increasing the surface area of graphene might enhance the interfacial interaction of graphene/epoxy composites. Recently, it has been verified that chemical activation using alkali compounds such as KOH and NaOH could obtain the activated graphene with higher specific surface area (SSA), a maximum SSA of 3100 m^2/g and well-developed porosity.[16–18] It is expected that activated graphene with higher SSA and pore volume than graphene might enhance the mechanical interaction and Van der Waals binding between graphene and epoxy which would generate the enhanced mechanical properties of epoxy nanocomposites.

In this work, we prepared activated thermally exfoliated graphene nanosheets (a-TEG) with higher SSA and pore volume and size than thermally exfoliated graphene nanosheets (TEG) by chemical activation, and compared epoxy nanocomposites with a-TEG and TEG which differed in their surface area and pore volume and size but had similar thicknesses. The microstructure and morphologies of TEG and a-TEG were obtained by X-ray diffraction (XRD) and atomic force microscope (AFM). Brunauer–Emmett–Teller (BET) method was used to get the SSA of TEG and a-TEG. The mechanical properties of neat epoxy and nanocomposites were evaluated by tensile, flexural, and dynamic mechanical tests.

EXPERIMENTAL

Materials

Epoxy (HS5382) based on bisphenol-A with an epoxy value of 0.45–0.50 was obtained from Guangdong Hai Xu Resin Factory, China. The curing agent, tetrahydrophthalic anhydride was purchased from Wenzhou Qingming Chemical, China. Graphite powders with an average diameter of 10 μm were purchased from Qingdao AoKe ShiMoCo, China. Chloroform, hydrochloric acid, potassium permanganate, concentrated sulfuric acid, and

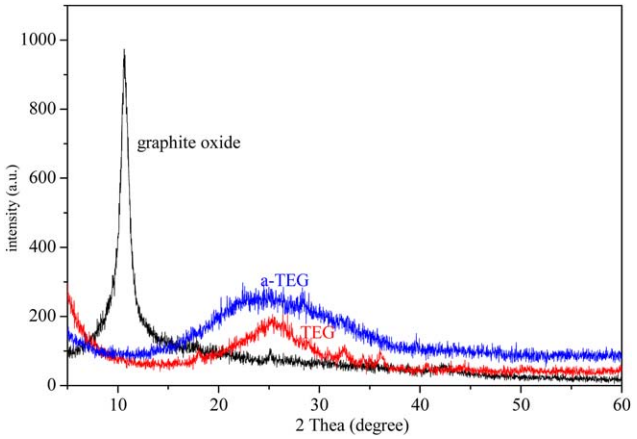

Figure 1. XRD analysis of graphite oxide, TEG, and a-TEG. [Color figure can be viewed in the online issue, which is available at wileyonlinelibrary.com.]

potassium hydroxide were purchased from Tianjin chemical factory and used as received.

Preparation and Activation of TEG

Graphite oxide was prepared using an improved Hummers method.[19,20] A 9 : 1 mixture of concentrated H_2SO_4/H_3PO_4 (360 : 40 mL) was added to a mixture of graphite powders (3.0 g, 1 wt equiv.) and $KMnO_4$ (18.0 g, 6 wt equiv.), producing a slight exothermal to 35–40°C. The mixture was stirred for 12 h at 50°C, forming a thick paste. Subsequently, it was cooled to room temperature and poured onto ice (400 mL) with 30% H_2O_2 (3 mL). The remaining solid materials were then washed in succession with deionized water until pH was 7. At last, they were dried 12 h by freeze drying to get graphite oxide (5.6 g).

Thermal reduction of graphite oxide is an effective approach that can be used to obtain bulk quantities of graphene.[21,22] Tube furnace was heated up to 1050°C and graphite oxide was rapidly exfoliated as well as reduced to obtain TEG in 30 s.[22] TEG (1 g) was then dispersed and soaked in aqueous KOH solution for 20 h ($KOH/TEG_{mass} = 6.5$) to obtain a maximum SSA for a-TEG.[18] The solid cake obtained after vacuum filtration of the excess KOH was dried. Then the solid cake in alumina combustion boat was put into the tube furnace with a nitrogen flow of 500 mL/min.[17] In addition, the activation temperature was maintained at 800°C.[23] At last, the a-TEG with excess reactant was washed by deionized water and dried for 15 h by freeze drying, to get final product a-TEG (0.7 g).

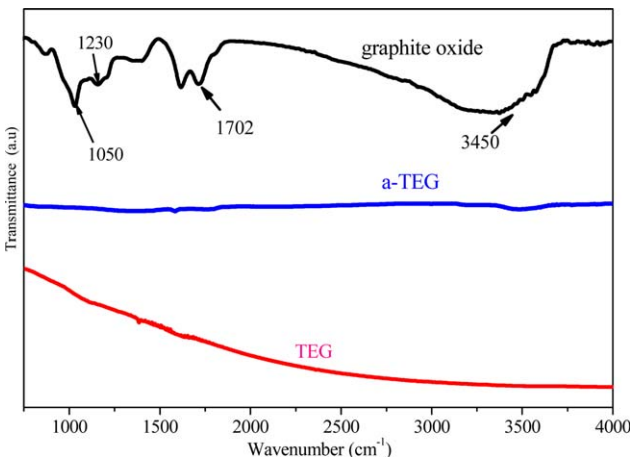

Figure 2. FTIR spectra of graphite oxide, TEG, and a-TEG. [Color figure can be viewed in the online issue, which is available at wileyonlinelibrary.com.]

Preparation of TEG/Epoxy and a-TEG/Epoxy Nanocomposites

The dispersion of carbon nanoparticles in chloroform as a route to obtain epoxy matrix composites was reported in literature.[24–26] Moreover, the technique based on the dispersion of graphene–chloroform suspension in the epoxy monomer is more appropriate.[27] Therefore, TEG and a-TEG were dispersed in chloroform to obtain epoxy nanocomposites in this study. Preparation of TEG/epoxy and a-TEG/epoxy composites was done following the protocol: (1) the prepared TEG and a-TEG were dispersed into chloroform to form a suspension of 0.1 g/100 mL followed by ultrasonication for 2 h, respectively (2) The epoxy with 70 wt % curing agent was mixed with the solution, following the stirring and ultrasonication for another 5 h at 60°C respectively (3) 2-Ethyl-4-methylimidazol was added into the mixture and degassed for 2 h in vacuum drying oven at 60°C (4) The mixture was injected into the mould and cured at 90°C for 2 h followed by a post-curing step at 120°C for 2 h and 150°C for 4 h (5) After curing, the samples were cooled naturally to room temperature. Finally, the epoxy nanocomposites containing graphene with weight fractions of 0.02, 0.05, 0.1, 0.2, and 0.5% were prepared. The pure epoxy sample was also prepared under the same curing condition.

Characterizations

The phase purity of graphite oxide, TEG, and a-TEG was characterized by XRD on an X-ray diffract meter with Cu Kα radiation ($\lambda = 1.5418$ Å). Fourier transform infrared spectroscopy (FTIR) was recorded using a Nicolet 6700 spectrophotometer in KBr pellets. X-ray photoelectron spectroscopy (XPS) investigations were carried out with a PHI 5700 ESCA System with Al Kα (1486.6 eV) radiation to characterize changes of the chemical components of TEG and a-TEG samples and the pressure in the XPS analyzing vacuum chamber was less than 3×10^{-9} mbar. AFM observation of TEG and a-TEG was performed on a CSPM 5500 scanning probe microscope. The measurement of the nitrogen adsorption isotherms was done with a Quantachrome Nova 2200e at 77.4 K to obtain the specific surface area and pore characteristics of TEG and a-TEG. The TEG and a-TEG dispersed in acetone were dip-coated onto freshly cleaved mica surfaces before testing, respectively. SEM images of tensile fractured specimens were obtained on a Hitachi S-4800 field-emission SEM system (operated at 4 kV). The samples were coated with a conductive layer of gold. The dog-bone-shaped specimens were prepared for uniaxial tensile testing. The flexural specimens (50 mm in length, 10 mm in width, and 2.4 mm in thickness) were cut from the composites by using a water-cooled diamond saw. The three-point flexural and tensile tests were carried out by Instron (3369, USA) mechanical testing machine. At least five samples were tested to obtain average values. Dynamic mechanical analysis was performed on a Mettler Toledo 861e instrument at 1 Hz frequency in flexural configuration. The loss factor (tanδ) and elastic modulus (E0) were

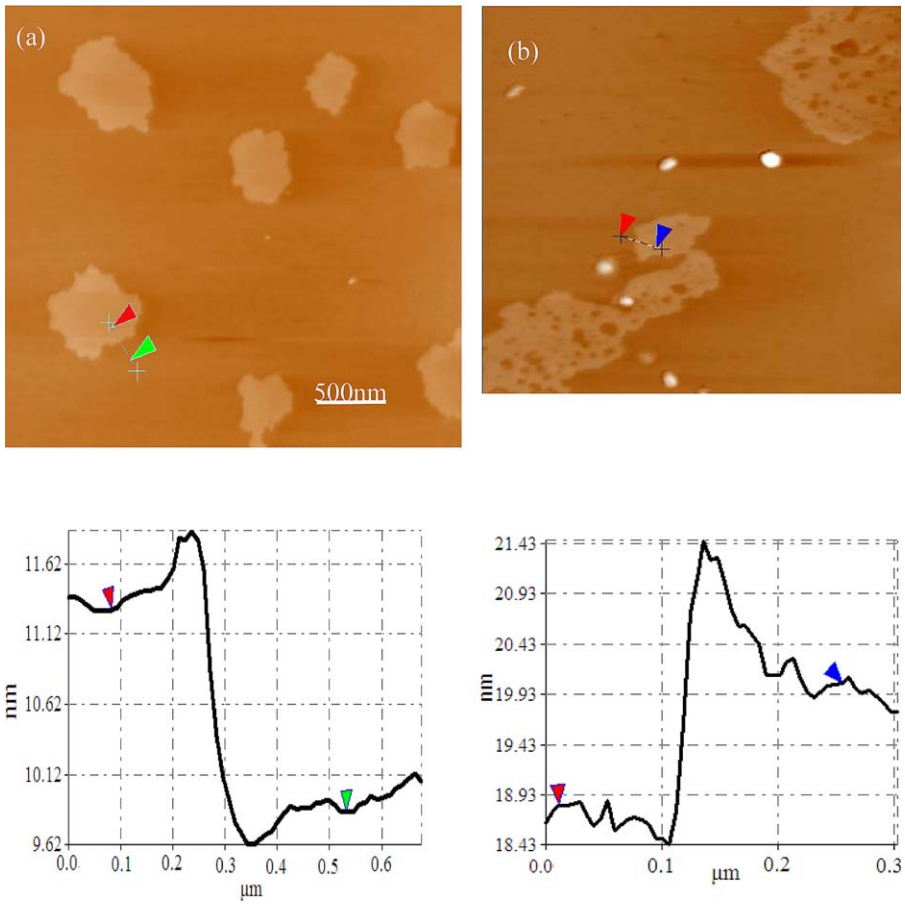

Figure 3. (a) AFM image of TEG dispersion in acetone on freshly cleaved mica surface through drop-casting, and height profile (below) along the black line indicating a sheet thickness of about 1.37 nm. (b) AFM image of a-TEG dispersion in acetone on freshly cleaved mica surface through drop-casting, and height profile (below) along the black line indicating a sheet thickness of about 1.22 nm. [Color figure can be viewed in the online issue, which is available at wileyonlinelibrary.com.]

measured from room temperature to 210°C. The experimental error was below 5%.

RESULTS AND DISCUSSION

Microstructure and Morphology of TEG and a-TEG

In the first step of this study, graphite oxide, TEG and a-TEG were characterized. Figure 1 reported the XRD analysis of graphite oxide, TEG and a-TEG. A relatively low peak at $2\theta = 10.7°$ obtained for graphite oxide corresponded to the diffraction of the graphite oxide plane. The *d*-spacing of graphite oxide can be calculated according to the Bragg's law:

$$n\lambda = 2d \sin \theta \quad (1)$$

where n is the diffraction series, λ is the X-ray wavelength, and *d* is the interlayer spacing of graphite oxide. The calculated value of *d* was 0.822 nm, implying that the sample was expanded when graphite was oxidized. However, the peak disappeared for TEG, indicating that the TEG layers were disordered.[28] In other words, TEG was successfully exfoliated. In addition, for TEG, the peak at 26° related to a *d*-spacing of 0.335 nm which was similar to the interlayer spacing of graphite, confirmed that TEG was reduced and not in an oxidative state. The results demonstrated that TEG with few layers was successfully prepared. In addition, the peak of a-TEG at 26° was dramatically broadened in comparison to that of TEG. It indicated that a-TEG displayed much less graphitic characteristics than TEG due to the collapse and destroying of carbon skeleton in the activated reaction[23].

FTIR spectra of graphite oxide, TEG, and a-TEG were presented in Figure 2. The results from FTIR revealed that the characteristic bands of graphite oxide were observed at 1050 and 3450 cm^{-1}(C—O and O—H stretching peak, respectively), 1702 cm^{-1} (C═O stretching in carboxylic acid group), and 1230 cm^{-1} (C—O stretching in epoxy group).[29,30] After graphite oxide was reduced to TEG, these residual oxygenic groups were removed, and thus the absorbance peak at 1050, 3450, 1702, and 1230 cm^{-1} disappeared in the TEG spectrum. In addition, the FTIR spectrum of a-TEG was similar to those of TEG. The results indicated that TEG and a-TEG were both reduced successfully. The carbon level of samples was changed from 91.12% to 91.90% after activation determined by XPS. The difference between TEG and a-TEG on element was negligible. Therefore, the similar elementhad no influence on the SSA of material and the mechanical properties of nanocomposites.

AFM was employed to determine the morphology of the TEG and a-TEG. A representative AFM image of TEG was shown in

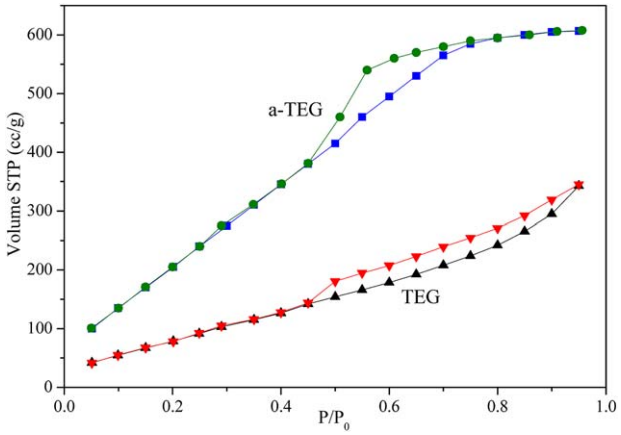

Figure 4. N_2 adsorption/desorption isotherms of TEG and a-TEG. [Color figure can be viewed in the online issue, which is available at wileyonlinelibrary.com.]

Figure 3(a), which revealed the presence of TEG with uniform thickness 1.37 nm. Figure 3(b) indicated that a-TEG was irregularly shaped and endowed with many nano-scale pores and an average thickness of around 1.22 nm.

The N_2 adsorption/desorption isotherms of TEG and a-TEG were shown in Figure 4. Compared with TEG, a-TEG was found to have typical IV isotherm curves indicating a micromesoporous structure.[23] Graphene had a high SSA (550 m^2/g) with the linear relative pressure ranging from 0.05 to 0.30. Activated TEG had a higher SSA with 1000 m^2/g than TEG. However, the SSA of a-TEG was lower than that in literature[18] because of the different methods for the preparation of graphene.

The obtained pore-size distribution of TEG and a-TEG was shown in Figure 5. It revealed the presence of micro pores with about 1nm size range as well as narrow mesopores centered 2–4 nm in a-TEG compared with TEG with some less than 1 nm micro pores. The results were in good agreement with the literature.[31]

The Mechanical Properties of Nanocomposites

The Tensile Properties of Nanocomposites. The uniaxial tensile results of the neat epoxy and nanocomposite samples were

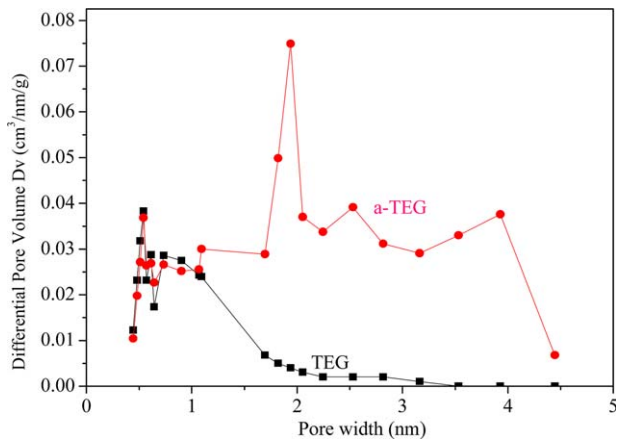

Figure 5. Pore size distributions of TEG and a-TEG. [Color figure can be viewed in the online issue, which is available at wileyonlinelibrary.com.]

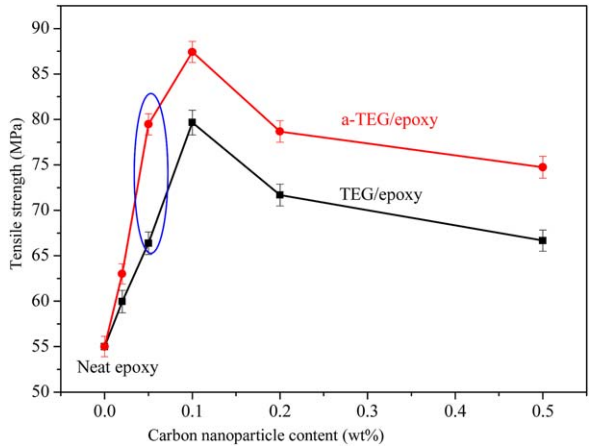

Figure 6. Tensile strength and modulus of nanocomposites at different contents of carbon nanoparticles. [Color figure can be viewed in the online issue, which is available at wileyonlinelibrary.com.]

shown in Figure 6. The obvious increase in the tensile properties was observed: the tensile strength of nanocomposites increased initially with increasing the TEG content and attained the maximum value at the 0.1 wt % TEG content corresponding to an increase of 42% compared with the pure epoxy. Afterwards, the composite strength decreased with further increasing the TEG content. The results were in good agreement with the literature.[32] A possible strengthening mechanism of TEG was the fact that the wrinkled surface of TEG at the nanoscale likely results in an enhanced mechanical interaction with the epoxy chains and, consequently, a strong interaction.[5,33,34] However, the excess TEG might be agglomerated, resulting in the formation of stress concentration sites in nanocomposites. Thus, the tensile strength of nanocomposites decreased with the further increasing of TEG content.

Further benefits to tensile strength were realized on a-TEG and a-TEG composites. It was clear that the reinforcing capability of a-TEG was much higher than that of TEG for all concentrations. Although the tensile strength of a-TEG/epoxy attained the

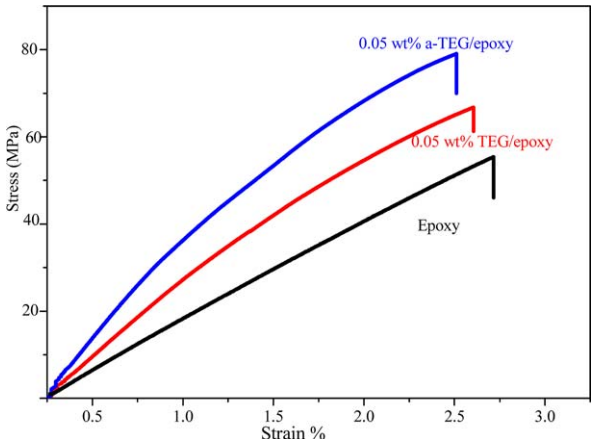

Figure 7. Stress–strain curves for neat epoxy, 0.05 wt % TEG/epoxy and 0.05 wt % a-TEG/epoxy. [Color figure can be viewed in the online issue, which is available at wileyonlinelibrary.com.]

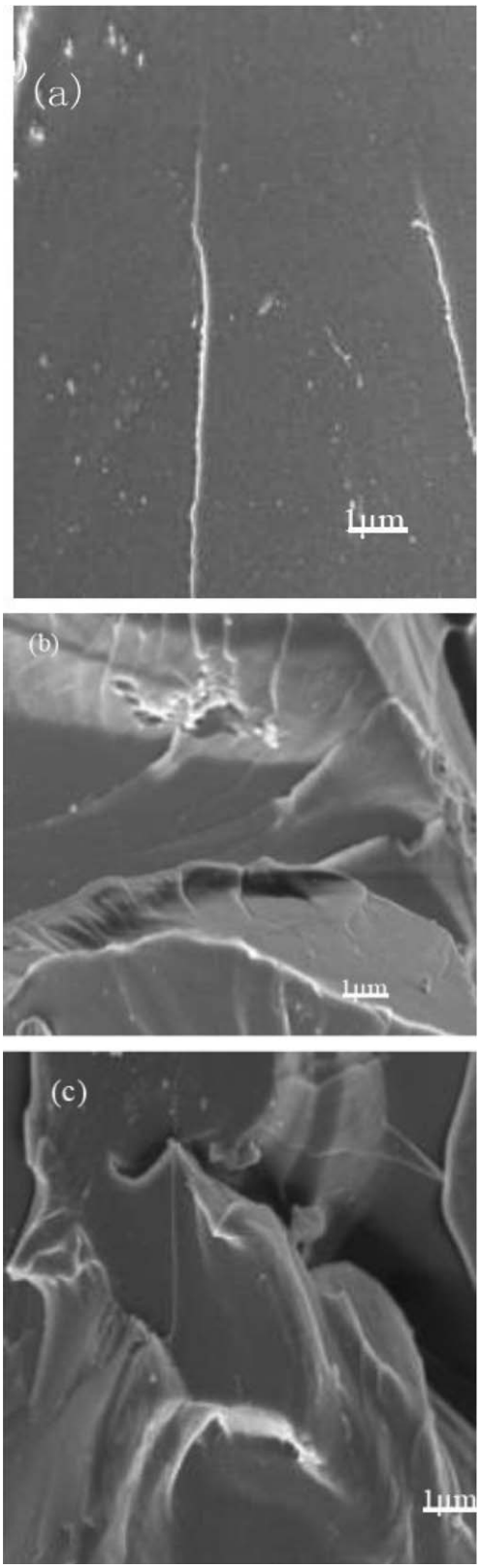

Figure 8. SEM images of the fractured surfaces (a) neat epoxy (b) 0.05 wt % TEG/epoxy nanocomposites (c) 0.05 wt % a-TEG /epoxy nanocomposites.

maximum value (87.9 MPa) at the 0.1 wt %, the difference between the tensile strength for a-TEG/epoxy and TEG/epoxy reached the maximum at 0.05 wt %. In detail, the tensile strength of a-TEG/epoxy was enhanced by up to 20% in comparison to that of TEG/epoxy at 0.05 wt %. Figure 7 was the stress–strain curves for neat epoxy, 0.05 wt % TEG/epoxy and 0.05 wt % a-TEG/epoxy nanocomposites. Compared with neat epoxy, the tensile stress of 0.05 wt % TEG/epoxy and a-TEG/epoxy nanocomposites increased while the elongation was reduced. Such a phenomenon was also observed in other reports.[34] It indicated that the stiffness and modulus of nanocomposites were higher than neat epoxy and 0.05 wt % a-TEG/epoxy showed a better reinforcing capability than TEG/epoxy. The reason why a-TEG/epoxy composites exhibited higher strength than its TEG counterpart might be attributed to two aspects. On one hand, the higher SSA of a-TEG increased the contact area and Van der Waals binding with epoxy, and made the stress transfer from epoxy to the carbon nanoparticles more effectively, compared with TEG. On the other hand, the chains of epoxy might stretch into the pore of a-TEG, enhancing mechanical interaction between epoxy and carbon nanoparticles.

When the content of carbon nanoparticles was 0.05 wt %, the disparities between the tensile strength of a-TEG/epoxy and TEG/epoxy reached the maximum. So we investigated and compared the interfacial properties of a-TEG/epoxy and TEG/epoxy nanocomposites further at the low content, 0.05 wt %. The following study was focused on comparing the flexural properties and dynamic mechanical results of a-TEG/epoxy and TEG/epoxy nanocomposites at 0.05 wt %. To confirm the morphological features of TEG and a-TEG in the epoxy, SEM images of the fractured surfaces for nanocomposites at 0.05 wt % were examined, as can be seen in Figure 8. The fractured surface of pure epoxy was quite even and smooth, indicating a typical brittle failure [Figure 8(a)]. However, nanocomposite fractures [Figure 8(b,c)] implied that more energy was needed to break the sample, and it is believed that the introduction of carbon nanoparticles leads to the change of section morphology and influence on the mechanical properties of composites.[35] In addition, the fracture surface of a-TEG/epoxy nanocomposites [Figure 8(c)] was much rougher than that of TEG/epoxy [Figure 8(b)] nanocomposites, indicating an increased interfacial interaction with epoxy.

The Flexural Properties of Nanocomposites. On the basis of the experimental load–deflection curves, the flexural strength and flexural modulus of neat epoxy and nanocomposites at 0.05 wt % could be extracted. As shown in Figure 9, the results indicated clearly that all samples with carbon nanoparticles showed a significant improvement in flexural properties compared with neat epoxy samples. This can be contributed to the fact that the introduction of carbon nanoparticles in epoxy could optimize the stress transfer from the polymer, dissipate the strain energy, prevent the failure of composites and lead to the high value of work of fracture. In addition, the flexural strength of a-TEG nanocomposites was increased by 50% in comparison to TEG nanocomposites, which indicated that the interfacial properties of nanocomposites were enhanced owing to the high mechanical interaction and Van der Waals binding between epoxy and a-TEG. However, the flexural modulus of TEG nanocomposites and a-TEG nanocomposites increased

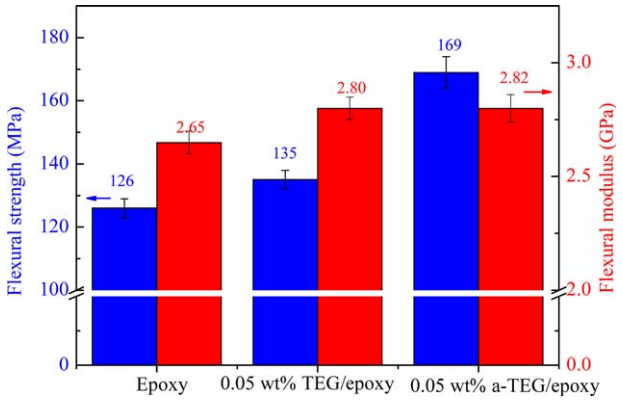

Figure 9. Flexural strength and modulus of neat epoxy and nanocomposites. [Color figure can be viewed in the online issue, which is available at wileyonlinelibrary.com.]

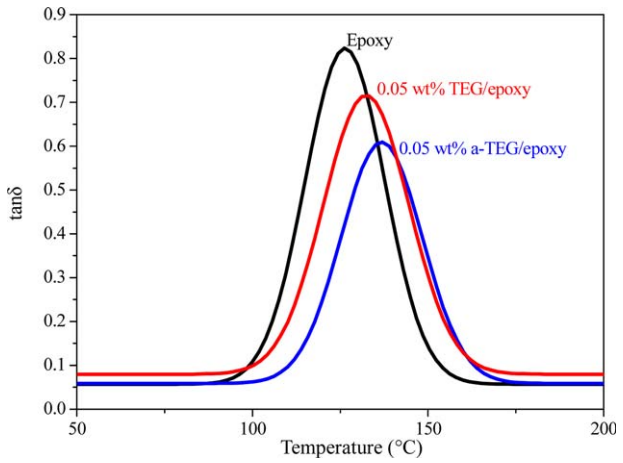

Figure 10. Damping factor (tanδ) and glass transition (T_g) of neat epoxy and nanocomposites. [Color figure can be viewed in the online issue, which is available at wileyonlinelibrary.com.]

marginally in comparison to that of epoxy. This is mainly due to the fact that the modulus of graphene nanosheets was much higher than epoxy, but the content of carbon nanoparticles was limited.[36,37]

Dynamic Mechanical Analysis of Nanocomposites. Viscoelastic characterization, glass transition temperature and damping values, of neat epoxy, and nanocomposites at 0.05 wt % were carried out by DMA analyses. Figure 10 showed the tanδ curves as a function of temperature for the different prepared materials. It is possible to observe that nanocomposites showed always higher T_g values in comparing to the neat cured epoxy, evidenced by the shift of the maximum of tanδ peaks, together with a decrease of the damping. It is well known that in particulate-filled polymers, the addition of rigid fillers can hinder the polymer chain movements and improve the crosslink density, leading to a damping decrement and a shift of T_g values to higher temperatures.[32,38] In this study, a significant reduction of damping (here evaluated as $\tan\delta_{max}$) was observed in the nanocomposites, together with a strong increment in T_g values. These changes in both T_g and damping are generally attributed to a strong filler-matrix interface. The interface bonding strength can be indirectly shown by a parameter α which was calculated according to the formula:

$$\alpha = ((\tan\delta_{max})_m - (\tan\delta_{max})_c)/V_f \quad (2)$$

where V_f is the volume fraction of reinforcement, and $(\tan\delta_{max})_m$ is the maximum tanδ peaks of epoxy matrix, and $(\tan\delta_{max})_c$ is the maximum tanδ peaks of composites.[39] In this formula, we considered TEG and a-TEG as the same V_f because of the similar density and the same weight. Thus, the α value of a-TEG/epoxy nanocomposites would be higher than that of TEG/epoxy nanocomposites in this formula due to the fact that the $(\tan\delta_{max})_c$ value of a-TEG/epoxy nanocomposites was lower than that of TEG/epoxy nanocomposites as shown in Figure 10. The results indicated that the interfacial interaction of a-TEG/epoxy was stronger than that of TEG/epoxy because of the mechanical bonding and Van der Waals binding between a-TEG and epoxy chains.

As shown in Figure11(a), the storage modulus of nanocomposites at glassy region (50°C) was increased in comparison to neat epoxy owing to the addition of carbon nanoparticles.[38] Moreover, the storage modulus of a-TEG/epoxy nanocomposites was higher than TEG/epoxy nanocomposites and neat epoxy. The results were in agreement with the results of Young's modulus and flexural modulus. In addition, a slight increase in the

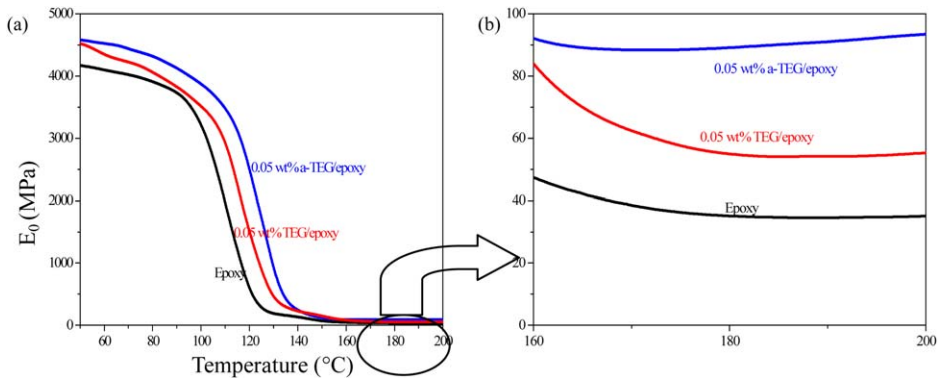

Figure 11. Storage modulus (E_0) of neat epoxy and nanocomposites. [Color figure can be viewed in the online issue, which is available at wileyonlinelibrary.com.]

rubbery modulus (between 160°C and 200°C) of nanocomposites [Figure 11(b)] was found compared with neat epoxy, and this increase effect of rubbery modulus for a-TEG/epoxy was more evident than that of TEG/epoxy. This can be attributed to the fact that carbon nanoparticles have a much higher modulus than epoxy matrix, resulting in a relatively higher molecular motion and higher amplitude of this motion in the rubbery region.[40]

CONCLUSIONS

In summary, a-TEG with higher SSA (1000 m^2/g) and more 2-4 nm mesopores than TEG was prepared by chemical activation successfully. In addition, a-TEG/epoxy nanocomposites was prepared by solvent methods and compared with TEG/epoxy nanocomposites and neat epoxy. The tensile strength of a-TEG/epoxy was increased by 20% in comparison to TEG/epoxy at 0.05 wt %. The flexural strength of a-TEG/epoxy nanocomposites was increased by 50% compared with that of TEG/epoxy nanocomposites at 0.05% graphene content. The results might be related to the fact that the interfacial interaction of a-TEG/epoxy nanocomposites was enhanced owing to their higher SSA and pore size compared with those of TEG. Consequently, the activation for pore introduction in graphene plane is a promising method for enhancing the mechanical properties of carbon nanoparticle/epoxy composites.

ACKNOWLEDGMENTS

The work was funded by the National Natural Science Foundation of China (U1362108, 11175130), Natural Science Foundation of Tianjin, China (10JCYBJC02300) and the National High Technology Research and Development Program of China (2012AA03A203).

REFERENCES

1. Zhao, J.; Wang, X.; Zhou, W.; Zhi, E.; Zhang, W.; Ji, J. *J. Appl. Polym. Sci.* **2013**, *130*, 3212.
2. Liang, J.; Huang, Y.; Zhang, L.; Wang, Y.; Ma, Y.; Guo, T.; Chen, Y. *Adv. Funct. Mater.* **2009**, *19*, 2297.
3. Ansari, S.; Neelanchery, M. M.; Ushus, D. *J. Appl. Polym. Sci.* **2013**, *130*, 3902.
4. Zhou, W.; Wang, X.; Wang, P.; Zhang, W.; Ji, J. *J. Appl. Polym. Sci.* **2013**, *130*, 4075.
5. Rafiee, M. A.; Rafiee, J.; Wang, Z.; Song, H.; Yu, Z.-Z.; Koratkar, N. *ACS Nano.* **2009**, *3*, 3884.
6. Wang, X.; Xing, W. Y.; Zhang, P.; Song, L.; Yang, H. Y.; Hu, Y. *Compos. Sci. Technol.* **2012**, *72*, 737.
7. Ma, H. L.; Zhang, Y. W.; Hu, Q. H.; He, S. L.; Li, X. F.; Zhai, M. L.; Yu, Z. Z. *Mater. Lett.* **2013**, *102*, 15.
8. Linghui Meng, D. F.; Chunhua, Z.; Zaixing, J.; Yudong, H. *Appl. Surf. Sci.* **2013**, *273*, 167.
9. Han, H. S.; You, J. M.; Jeong, H.; Jeon, S. *Appl. Surf. Sci.* **2013**, *284*, 438.
10. Yang, H. F.; Li, F. H.; Shan, C. S.; Han, D. X.; Zhang, Q. X.; Niu, L.; Ivaska, A. *J. Mater. Chem.* **2009**, *19*, 4632.
11. Du Ngoc Uy, L.; Abu Bakar, A.; Azahari, B.; Ariff, Z. M.; Chujo, Y. *Polym. Test.* **2012**, *31*, 931.
12. Zhang, Y.; Yao, H.; Ortiz, C.; Xu, J.; Dao, M. *J. Mech. Behav. Biomed.* **2012**, *15*, 70.
13. Jana, S.; Zhong, W. H. *Mater. Sci. Eng.* **2009**, *525*, 138.
14. Chatterjee, S.; Nafezarefi, F.; Tai, N. H.; Schlagenhauf, L.; Nueesch, F. A.; Chu, B. T. T. *Carbon* **2012**, *50*, 5380.
15. El Achaby, M.; Qaiss, A. *Mater. Des.* **2013**, *44*, 81.
16. Molina-Sabio, M.; Rodriguez-Reinoso, F. *Colloids. Surf.* **2004**, *241*, 15.
17. Lillo-Rodenas, M. A.; Cazorla-Amoros, D.; Linares-Solano, A. *Carbon* **2003**, *41*, 267.
18. Murali, S.; Potts, J. R.; Stoller, S.; Park, J.; Stoner, M. D.; Zhang, L. L.; Zhu, Y.; Ruoff, R. S. *Carbon* **2012**, *50*, 3482.
19. Marcano, D. C.; Kosynkin, D. V.; Berlin, J. M.; Sinitskii, A.; Sun, Z.; Slesarev, A.; Alemany, L. B.; Lu, W.; Tour, J. M. *ACS Nano* **2010**, *4*, 4806.
20. Chengbo, S.; Lei, C.; Zhiwei, X.; Yanan, J.; Yinglin, L.; Chunhong, W.; Mingjing, S.; Zhen, W.; Qiwei, G. *Physica E* **2012**, *44*, 1420.
21. Schniepp, H. C.; Li, J. L.; McAllister, M. J.; Sai, H.; Herrera-Alonso, M.; Adamson, D. H.; Prud'homme, R. K.; Car, R.; Saville, D. A.; Aksay, I. A. *J. Phys. Chem. B* **2006**, *110*, 8535.
22. McAllister, M. J.; Li, J.-L.; Adamson, D. H.; Schniepp, H. C.; Abdala, A. A.; Liu, J.; Herrera-Alonso, M.; Milius, D. L.; Car, R.; Prud'homme, R. K.; Aksay, I. A., *Chem. Mater.* **2007**, *19*, 4396.
23. Zhu, Y.; Murali, S.; Stoller, M. D.; Ganesh, K. J.; Cai, W.; Ferreira, P. J.; Pirkle, A.; Wallace, R. M.; Cychosz, K. A.; Thommes, M.; Su, D.; Stach, E. A.; Ruoff, R. S. *Science* **2010**, 332, 1537.
24. O'Neill, A.; Khan, U.; Nirmalraj, P. N.; Boland, J.; Coleman, J. N. *J. Phys. Chem. C* **2011**, *115*, 5422.
25. Prolongo, S. G.; Buron, M.; Gude, M. R.; Chaos-Moran, R.; Campo, M.; Urena, A. *Compos. Sci. Technol.* **2008**, *68*, 2722.
26. Biswas, S.; Fukushima, H.; Drzal, L. T. *Compos. A* **2011**, *42*, 371.
27. Monti, M.; Rallini, M.; Puglia, D.; Peponi, L.; Torre, L.; Kenny, J. M. *Compos. A* **2013**, *46*, 166.
28. Nguyen, D. A.; Lee, Y. R.; Raghu, A. V.; Jeong, H. M.; Shin, C. M.; Kim, B. K. *Polym. Int.* **2009**, *58*, 412.
29. Yang, H.; Li, F.; Shan, C.; Han, D.; Zhang, Q.; Niu, L.; Ivaska, A. *J. Mater. Chem.* **2009**, *19*, 4632.
30. Shim, S. H.; Kim, K. T.; Lee, J. U.; Jo, W. H. *ACS Appl. Mater. Interf.* **2012**, *4*, 4184.
31. Zhao, X.; Zhang, L. L.; Murali, S.; Stoller, M. D.; Zhang, Q. H.; Zhu, Y. W.; Ruoff, R. S. *Acs Nano* **2012**, *6*, 5404.
32. Martin-Gallego, M.; Hernandez, M.; Lorenzo, V.; Verdejo, R.; Lopez-Manchado, M. A.; Sangermano, M. *Polymer* **2012**, *53*, 1831.
33. Ramanathan, T.; Abdala, A. A.; Stankovich, S.; Dikin, D. A.; Herrera-Alonso, M.; Piner, R. D.; Adamson, D. H.;

Schniepp, H. C.; Chen, X.; Ruoff, R. S.; Nguyen, S. T.; Aksay, I. A.; Prud'homme, R. K.; Brinson, L. C. *Nat. Nanotech.* **2008**, *3*, 327.

34. Martin-Gallego, M.; Hernandez, M. M. B.; Verdejo, R.; Lopez-Manchado, M. A. *Eur. Polym. J.* **2013**, *49*, 1347.
35. Wang, J. L.; Shi, Z. X.; Ge, Y.; Wang, Y.; Fan, J. C.; Yin, J. *J. Mater. Chem.* **2012**, *22*, 17663.
36. Shen, X. J.; Liu, Y.; Xiao, H. M.; Feng, Q. P.; Yu, Z. Z.; Fu, S. Y. *Compos. Sci. Technol.* **2012**, *72*, 1581.
37. Min, C.; Zhou Shi, X. S. *Polym. Plast. Technol. Eng.* **2010**, *49*, 1172.
38. Gkikas, G.; Barkoula, N. M.; Paipetis, A. S. *Compos. B* **2012**, *43*, 2697.
39. Michio Ashida, T. N.; Mashimo, S. *J. Appl. Polym. Sci.* **1985**, *30*, 1011.
40. Rahman, M. M.; Zainuddin, S.; Hosur, M. V.; Robertson, C. J.; Kumar, A.; Trovillion, J.; Jeelani, S. *Compos. Struct.* **2013**, *95*, 213.